https://doi.org/10.5194/wes-2026-14
Preprint. Discussion started: 13 February 2026

eawe european academy of wind energy
Open Access WIND ENERGY SCIENCE DISCUSSIONS

Fast blockage models for wind-farm power prediction

Koen Devesse[1] and Johan Meyers[1]
[1]Department of Mechanical Engineering, KU Leuven, Leuven, Belgium
Correspondence: Koen Devesse (koen.devesse@kuleuven.be)

Abstract. Large offshore wind farms can trigger atmospheric gravity waves, with the associated hydrostatic blockage effect impacting their energy yield. Unfortunately, to date no tools exist that can model this wind-farm gravity-wave interaction and blockage at a computational cost that is not drastically higher than conventional engineering wake models. To address this, this paper applies insights from two-scale momentum (2SM) theory to an atmospheric perturbation model (APM), thereby significantly speeding up the latter. This leads to two different models, with one using pre-computed farm-level coefficients to compute the turbine forces and power output, while the other relies on repeated wake model evaluations. The core 2SM hypothesis and both developed models are validated using a prior LES dataset of a large wind farm. Both fast 2SM–APMs perform well, predicting blockage-corrected farm power at a computational cost that is only a factor 40 slower than a standalone wake model.

1 Introduction

As offshore wind turbines and farms continue to grow in both size and installed capacity, they reach the point where they form an obstacle to the entire atmospheric boundary layer (ABL). In conventionally neutral boundary layers (CNBLs), where a neutral ABL is topped by a capping inversion and a stratified upper atmosphere, they can trigger gravity waves, creating upstream pressure gradients and blockage effects that impact their performance (Bleeg et al., 2018; Allaerts and Meyers, 2017, 2018; Centurelli et al., 2021; Lanzilao and Meyers, 2022, 2023a, 2024; Maas, 2023a, b; Stipa et al., 2024b). As offshore wind turbines and farms continue to grow in size and capacity, these mesoscale effects are becoming more important to farm operation and planning.

Currently, conventional engineering tools rely on the superposition of individual turbine effects, thereby implicitly assuming that their aggregate effect is not larger than the sum of its parts (Porté-Agel et al., 2020). These *wake models* remain widely used because of their low computational cost, which makes them well-suited for farm planning, control, and annual energy production estimates. In contrast, computational fluid dynamics (CFD) methods like Reynolds-averaged Navier-Stokes (RANS), large-eddy simulations (LES), or mesoscale climate models are able to capture most of the relevant flow phenomena. However, their high cost prevents them from being widely used for fast farm power predictions (Meyers et al., 2022).

Installing and operating the next generation of offshore wind farms will require new models that can simulate atmospheric flow dynamics, while keeping the computational cost orders of magnitude below conventional CFD methods. One promising recently developed tool that fits these requirements is the atmospheric perturbation model (APM) (Allaerts and Meyers, 2019;

https://doi.org/10.5194/wes-2026-14
Preprint. Discussion started: 13 February 2026

eawe european academy of wind energy
Open Access WIND ENERGY SCIENCE DISCUSSIONS

Devesse et al., 2024a; Stipa et al., 2024a). Building on earlier work by Smith (2010), this model simulates the wind-farm atmosphere interaction explicitly, while coupling to conventional wake models for fast farm power predictions. However, it still has to repeatedly solve linear differential equations, resulting in a relatively high computational cost compared to standard wake models (several hundred to a thousand times slower, or approximately one to five minutes on a standard laptop) (Devesse et al., 2024b).

One way to further simplify and speed up the modeling of wind-farm atmosphere interactions is the two-scale momentum (2SM) framework introduced by Nishino and Dunstan (2020). At its core, this approach assumes a separation between the turbine- and farm-scale flows. As a result of this hypothesis, variations in farm power output due to mesoscale effects are fully determined by the associated changes in the average velocity over the farm. Based on high-fidelity LES results, this hypothesis has been confirmed for large wind farms in idealized conditions (Kirby et al., 2022, 2025).

Other recent studies have proposed wind farm models relying on the same idea of scale separation. Van der Laan et al. (2023) and Stipa et al. (2024c) proposed actuator-farm models for RANS and LES, respectively, allowing these methods to simulate wind farms without resolving the turbine-scale flow. Similarly, Du et al. (2025) developed a wind-farm parametrization for mesoscale weather models, which due to their kilometer-scale resolution cannot represent individual turbines, based on matching the average velocity in the farm between the mesoscale model and a wake model. However, since these studies are not as explicit in their theoretical treatment of this scale separation, we will refer to the overall idea as the two-scale momentum approach, following Nishino and Dunstan (2020).

The goal of the current paper is to combine the 2SM and APM approaches, leveraging insights from the former to speed up and simplify the latter. Since the 2SM hypothesis states that a farm's power output only depends on the average velocity in the farm, the APM may neglect the variations in the turbine force within the farm induced by gravity wave effects. Due to the linear nature of the APM, this transforms the model's governing equations into a system of scalar equations, drastically lowering its computational cost. We use this to develop two versions of the sped-up APM, one which uses farm thrust and power coefficients to model the farm, following earlier 2SM studies, and one which couples directly to a standard wake model. Both models are validated using the LES dataset of a large wind farm operating in CNBL conditions from Lanzilao and Meyers (2024).

The remainder of this paper is outlined as follows. Section 2 provides an overview of 2SM theory, and demonstrates its core hypothesis using the LES results of Lanzilao and Meyers (2024). Section 3 then introduces the APM's governing equations and how they are solved. Combining these two, section 4 shows how a 2SM–APM can cheaply calculate a farm's power output if its farm-level thrust and power coefficients are known. Building on this, section 5 develops an alternative method that couples the farm-averaged APM output directly to a wake model, thereby eliminating the need for these farm coefficients but requiring repeated wake model evaluations. Finally, section 6 gives an overview of the results and an outlook for future research.

https://doi.org/10.5194/wes-2026-14
Preprint. Discussion started: 13 February 2026

eawe european academy of wind energy
Open Access WIND ENERGY SCIENCE DISCUSSIONS

2 Two-scale Momentum Theory

Recently, Kirby et al. (2025) demonstrated that the 2SM theory developed by Nishino and Dunstan (2020) can be used to simplify the interaction between mesoscale atmospheric flows and wind farm operation. The core hypothesis of 2SM theory is a separation of internal and external effects and the associated spatial scales. Internal effects, such as turbine setpoints and wakes, determine the ratios of the individual turbine disk velocities S_k to the average streamwise velocity U_f in the farm region. External effects, such as large-scale momentum advection, entrainment above the farm, or gravity-wave-induced pressure gradients, act on the farm scale, and affect the average velocity within the farm U_f. The total farm power P_f can then be expressed as

$$P_f = C_p^* \frac{\rho U_f^3}{2} A_f, \quad C_p^* = \sum_{k=1}^{N_t} C'_{p,k} \frac{S_k^3}{U_f^3} \frac{A_k}{A_f}, \quad A_f = \sum_{k=1}^{N_t} A_k, \tag{1}$$

where ρ is the air density, A_f is the total rotor area of the farm turbines, C_p^* is the internal farm power coefficient, N_t is the number of turbines, and A_k and $C'_{p,k}$ are the turbine disk areas and disk-based power coefficients, respectively, with k indicating the turbine number.

Nishino and Dunstan (2020) make an analogous argument for the farm thrust, so that

$$F = C_T^* \frac{U_f^2}{2} A_f, \quad C_T^* = \sum_{k=1}^{N_t} C'_{T,k} \frac{S_k^2}{U_f^2} \frac{A_k}{A_f}, \tag{2}$$

where F is the total farm force (scaled with air density), C_T^* is the farm thrust coefficient, and $C'_{T,k}$ are the disk-based turbine thrust coefficients. Like C_p^*, the internal farm thrust coefficient C_T^* is assumed to only depend on the internal problem.

Earlier work by Kirby et al. (2025) has shown that the internal power coefficient C_p^* as defined in equation (1) is a good heuristic for internal effects. The 2SM hypothesis then implies that C_p^* can be calculated using neutral flow simulations of the same farm or engineering wake models, while the problem of including mesoscale stratification effects in farm power calculations is simplified to solving only the external problem, i.e. estimating U_f.

We demonstrate this by taking C_p^* from a neutral flow simulation, and U_f from different CNBL simulations with different meso-scale stratification effects, but the same farm layout. For this, we use the prior LES dataset from Lanzilao and Meyers (2024), which consists of 36 simulations of the same large wind farm (Lanzilao and Meyers, 2023b). This farm has 160 10MW turbines, arranged in a uniform staggered layout. Each simulation has a different combination of boundary layer heights H, capping inversion strengths $\Delta\theta$, and atmospheric lapse rates Γ. The different cases are identified with these parameters, so that $H500$-$\Delta\theta5$-$\Gamma4$ denotes the case with the precursor profile initialized with these values. For each boundary layer height, the dataset also includes a truly neutral wind-farm simulation. A detailed description of the LES setup and results is given by Lanzilao and Meyers (2024).

We set the height H_f of the volume over which the farm average is defined equal to twice the turbine hub height z_h. This height is above the turbine tip height but below the ABL height for all the cases in the dataset of Lanzilao and Meyers (2024). Note that this is not the same height as was used in previous 2SM studies (Nishino and Dunstan, 2020; Kirby et al., 2022, 2025),

https://doi.org/10.5194/wes-2026-14
Preprint. Discussion started: 13 February 2026

eawe european academy of wind energy
Open Access WIND ENERGY SCIENCE DISCUSSIONS

Table 1. Specification of the 2SM farm averaging volume for the cases of Lanzilao and Meyers (2024).

Dimension	Value
Height H_f	238 m
Length	14.85 km
Width	9.603 km

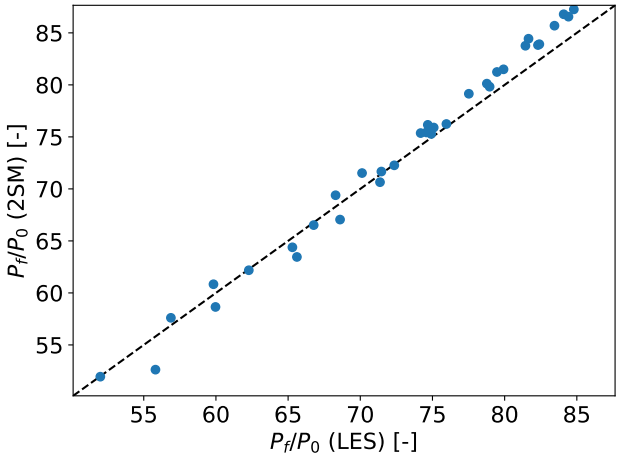

Figure 1. A comparison of farm power P_f as calculated by LES (x-axis) and equation 1 (y-axis) for all 36 CNBL cases from the dataset by Lanzilao and Meyers (2024), scaled with the power outputs of standalone turbine simulations P_0. The power coefficient C_p^* is calculated using a neutral flow simulation (i.e. case $H500$-$\Delta\theta0$-$\Gamma0$ from the same dataset).

where consistently $H_f = 2.5z_h$. However, we believe the lower height yields better results, as it aligns more closely with the region relevant to turbine-scale flow. It also does not stick out into the free atmosphere for the cases with very shallow boundary layers, whereas the higher one does. This probably explains why we find C_p^* to be consistent across all cases, whereas Kirby et al. (2025) found that the farm coefficients change for the lowest capping inversions. Finally, we also use a slightly wider averaging volume to avoid leaving out parts of the disks at the edges of the farm. The exact dimensions of the resulting control volume are listed in table 1.

To calculate C_p^*, we use the 3D time-averaged velocity fields of case $H500$-$\Delta\theta0$-$\Gamma0$. After averaging the streamwise velocity field to obtain U_f, we obtain C_p^* from equation 1. Subsequently, the farm power for the other cases are calculated by averaging their U_f and combining it with the prior C_p^* through equation 1. The resulting power outputs are scaled with the power output of a standalone turbine P_0 to avoid issues with the power calculation in LES related to the used actuator-disk method and grid size, as was done by Lanzilao and Meyers (2024). The results are shown in figure 1. The root-mean square error (RMSE) on P_f is 1% of the farm installed capacity, showing that under idealized conditions the 2SM assumption yields good results.

https://doi.org/10.5194/wes-2026-14
Preprint. Discussion started: 13 February 2026

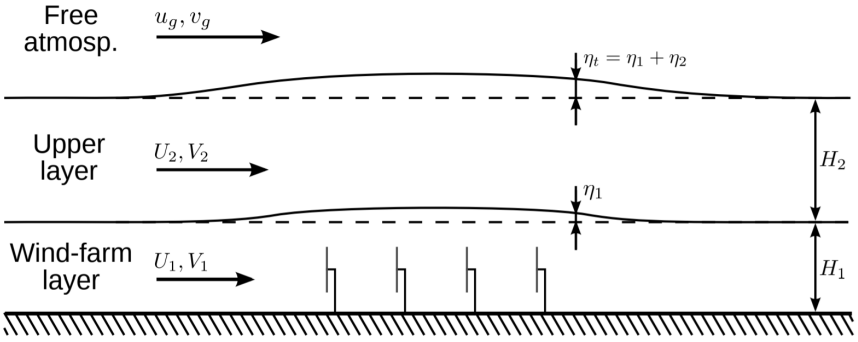

Figure 2. Schematic representation of the atmospheric perturbation model. Figure reproduced from D. Allaerts and J. Meyers, Sensitivity and feedback of wind-farm-induced gravity waves, Journal of Fluid Mechanics, 862, 990-1028 (2019).

3 Atmospheric Perturbation Model

If C_P^* and C_T^* are known, calculating the farm power output with the 2SM approach then comes down to finding the average farm velocity U_f. The APM is well-suited for this, as it is a fast model for mesoscale atmosphere–farm interaction. Therefore, this section presents a brief overview of the APM.

The APM is a simplified model, and treats the ABL as two layers of vertically averaged flow, separated by a pliant surface (Allaerts and Meyers, 2019). In each of these layers, the continuity and horizontal momentum equations are solved explicitly for the average velocities and layer thicknesses. The wind-farm forces are added in the momentum equations for the lower layer, also called the wind-farm layer, while only affecting the upper layer via interactions through the pliant surface. The resulting model structure is visualized in figure 2.

The main advantage of the APM is that the vertical averaging drastically lowers the computational cost of the model compared to conventional simulation tools, since it essentially reduces the vertical resolution to the ABL height. The horizontal resolution is likewise reduced by applying a Gaussian filter with a kernel size of 1 km (Allaerts and Meyers, 2019; Devesse et al., 2024a).

Mathematically, the APM can be derived by applying these filtering and height-averaging operators to the flow. For example, the lower layer velocity is defined as (Devesse et al., 2024a)

$$\langle \widetilde{\boldsymbol{u}} \rangle_1 = \frac{1}{h_1} \int_0^{h_1} \iint_{L_x \times L_y} G_\ell(x - x', y - y') \boldsymbol{u}(x', y', z) \mathrm{d}x' \mathrm{d}y' \mathrm{d}z, \tag{3}$$

where the subscript 1 indicates the lower layer, the angled brackets and tilde denote the height-averaging and filtering, respectively, $\boldsymbol{u}$ is the horizontal velocity vector, h_1 is the lower layer thickness, $L_x \times L_y$ is the APM domain size, and G_ℓ is a Gaussian kernel with filter length $\ell = 1\mathrm{km}$. The flow is then further linearized around a uniform background state, so that for the lower layer

$$\langle \widetilde{\boldsymbol{u}} \rangle_1 = \boldsymbol{U}_1 + \boldsymbol{u}_1', \quad h_1 = H_1 + \eta_1, \tag{4}$$

https://doi.org/10.5194/wes-2026-14
Preprint. Discussion started: 13 February 2026

eawe european academy of wind energy
Open Access WIND ENERGY SCIENCE DISCUSSIONS

where $\boldsymbol{U}_1$ and H_1 are the layer velocity and thickness in the absence of the wind farm, and $\boldsymbol{u}_1'$ and η_1 are the perturbations to this state. For the upper layer, the notation is analogous.

The governing equations of the model can then be found by applying the above operators to the incompressible Reynolds-averaged steady-state Navier-Stokes equations, and linearizing the result. Thorough descriptions of this procedure can be found in Allaerts and Meyers (2019) and Devesse et al. (2024a). The resulting set of equations is

$$\boldsymbol{U}_1 \cdot \nabla_h \eta_1 + H_1 \nabla_h \cdot \boldsymbol{u}_1' = 0, \tag{5}$$

$$\boldsymbol{U}_2 \cdot \nabla_h \eta_2 + H_2 \nabla_h \cdot \boldsymbol{u}_2' = 0, \tag{6}$$

$$\begin{aligned} \boldsymbol{U}_1 \cdot \nabla_h \boldsymbol{u}_1' \quad = \quad & -\frac{1}{\rho}\nabla_h p' + f_c \mathbf{J} \cdot \boldsymbol{u}_1' \\ & + \nu_{t,1} \nabla_h^2 \boldsymbol{u}_1' + \frac{\mathbf{D}'}{H_1} \cdot \Delta_1^2 \boldsymbol{u}' - \frac{\mathbf{C}'}{H_1} \cdot \boldsymbol{u}_1' - \frac{\boldsymbol{T}_{h3,1} - \boldsymbol{T}_{h3,0}}{H_1^2}\eta_1 \\ & + \frac{\widetilde{\boldsymbol{f}}_{wf} + \widetilde{\Delta \boldsymbol{\tau}_{wf}}}{H_1 + \eta_1} + \nabla_h \cdot \langle \boldsymbol{\tau}_{d,hh} \rangle_1 , \end{aligned} \tag{7}$$

$$\begin{aligned} \boldsymbol{U}_2 \cdot \nabla_h \boldsymbol{u}_2' \quad = \quad & -\frac{1}{\rho}\nabla_h p' + f_c \mathbf{J} \cdot \boldsymbol{u}_2' + \nu_{t,2} \nabla_h^2 \boldsymbol{u}_2' - \frac{\mathbf{D}'}{H_2} \cdot \Delta_1^2 \boldsymbol{u}' + \frac{\boldsymbol{T}_{h3,1}}{H_2^2}\eta_2 \\ & - \frac{\widetilde{\Delta \boldsymbol{\tau}_{wf}}}{H_2 + \eta_2}, \end{aligned} \tag{8}$$

where the subscript h indicates horizontal vector components, p' is the pressure perturbation induced by gravity waves, ρ is the air density, f_c is the Coriolis parameter, $\mathbf{J}$ is the two-dimensional rotation dyadic, and ν_t are height-averaged eddy viscosities. Furthermore, $\boldsymbol{T}_{h3,0}$ and $\boldsymbol{T}_{h3,1}$ are the unperturbed turbulent shear stresses at the ground and the layer interface, respectively, and $\mathbf{C}'$ and $\mathbf{D}'$ are the Jacobians of these stresses to the layer velocities. Finally, $\boldsymbol{f}_{wf}$, $\Delta\boldsymbol{\tau}_{wf}$, and $\langle \boldsymbol{\tau}_{d,hh} \rangle_1$ are the perturbing effects of the wind farm, with $\boldsymbol{f}_{wf}$ denoting the turbine forces (scaled with air density), $\Delta\boldsymbol{\tau}_{wf}$ representing the shear stresses between the layers due to the added turbulence intensity caused by the farm, and $\langle \boldsymbol{\tau}_{d,hh} \rangle_1$ denoting dispersive stresses due to turbine-scale flow heterogeneity. For the sake of simplicity, the latter two are not included in this study.

The pressure perturbation in the ABL p' is caused by the gravity waves on the capping inversion and in the free atmosphere. These waves are themselves triggered by the displacement of the capping inversion $\eta_t = \eta_1 + \eta_2$. Their pressure feedback can be related to this displacement in Fourier space, so that (Smith, 2010)

$$\frac{p'}{\rho} = g' \eta_t + \mathcal{F}^{-1}(\Phi) * \eta_t, \tag{9}$$

where g' is the reduced gravity in the capping inversion, $\mathcal{F}^{-1}$ denotes an inverse Fourier transform, and $*$ denotes a convolution. Continuing, Φ are the stratification coefficients, which determine the pressure feedback of the internal gravity waves in the free atmosphere. For uniform barotropic free atmospheres, these coefficients are calculated in Fourier space as (Smith, 2010)

$$\Phi = \frac{\mathrm{i}\left(N_g^2 - \Omega^2\right)}{m} \tag{10}$$

https://doi.org/10.5194/wes-2026-14
Preprint. Discussion started: 13 February 2026

eawe european academy of wind energy
Open Access WIND ENERGY SCIENCE DISCUSSIONS

where $N_g = \sqrt{\frac{g}{\theta}\frac{\mathrm{d}\theta}{\mathrm{d}z}}$ is the Brunt-Väisälä frequency in the free atmosphere, and Ω is the intrinsic wave frequency. The vertical wavenumber m is given by the dispersion relation (Gill, 1982).

The grid spacing of the APM is significantly larger than the individual turbine diameters. Therefore, the turbine forces are considered to be point forces before they are filtered onto the numerical grid, so that the total force is simply a sum of Gaussians (Allaerts and Meyers, 2019):

$$\widetilde{\boldsymbol{f}}_{wf} = \sum_{k}^{N_t} G_{\ell,k} \boldsymbol{f}_k, \tag{11}$$

where each $G_{\ell,k}$ is a Gaussian kernel centered around turbine k, and the turbine thrusts f_k are (Allaerts and Meyers, 2019)

$$\boldsymbol{f}_k = \frac{1}{2} C'_{T,k} A_k S_k^2 \boldsymbol{e}_k, \tag{12}$$

where S_k and $\boldsymbol{e}_k$ are the turbine disk velocities and orientations, respectively. These turbine-level conditions depend on the APM state, so that throughout the farm there is a two-way coupling between the turbine forces and the mesoscale flow. Past studies incorporated this coupling by calculating S_k with a wake model, and modifying the wake model's background velocity to incorporate the mesoscale velocity fluctuations across the farm (Allaerts and Meyers, 2019; Stipa et al., 2024a; Devesse et al., 2024a, b). The goal of this work is to define a faster farm-averaged coupling method based on 2SM theory.

To incorporate the pressure feedback of the internal gravity waves, the system of equations 5-8 is solved with a Fourier-Galerkin method. All terms in equations 5-8 except the turbine forces $\widetilde{\boldsymbol{f}}_{wf}$ then decouple per wavenumber, so that for a given $\widetilde{\boldsymbol{f}}_{wf}$ the system can be easily solved through matrix inversion. The turbine forces are included through a fixed-point iteration, where at each step the linear APM equations are solved for a given forcing. The turbine forces $\widetilde{\boldsymbol{f}}_{wf}$ are then re-calculated based on the APM state, and the process is repeated until convergence. For details, see Devesse et al. (2024a).

4 Combining 2SM and APM

The 2SM approach simplifies the turbine-scale problem by relating the turbine forces and power outputs to only the average velocity in the farm through C_P^* and C_T^*. The most straightforward way of combining this with the APM is then to use the APM as the external model to find U_f, while using C_T^* and C_p^* to represent the turbine forces in the APM. This section focuses on developing such coupling and on leveraging the simplifications of 2SM theory to speed up the APM.

The goal of this section is use the APM to solve the external problem as cheaply as possible. Therefore, we treat the farm coefficients C_P^* and C_T^* as known inputs for now. However, their computation still represents an additional cost, associated with calculating the farm-averaged velocity in a prior (neutral) wake-model simulation. This will be addressed in section 5.2, using insights from the methods developed in this section.

We will build up the combination of the 2SM and APM approaches step by step. First, section 4.1 discusses the differences between the mathematical averaging operators used by 2SM theory and in the derivation of the APM, and bridges the gap between them. Then, section 4.2 sets up a simplified version of the APM focused on finding U_f, thereby leveraging the insights

https://doi.org/10.5194/wes-2026-14
Preprint. Discussion started: 13 February 2026

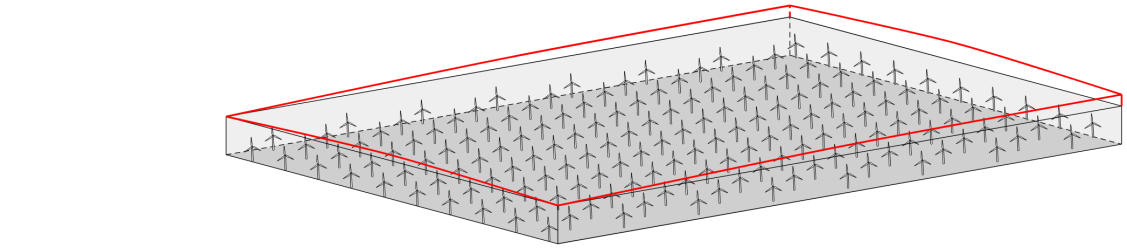

Figure 3. Sketch of the farm control volume (black) and lower APM layer (red) for a rectangular farm. Note that in contrast to the 2SM farm control volume, the upper boundary of the APM layer is not rigid, as it follows the streamlines.

of 2SM theory to speed up the model. Finally, section 4.3 validates the developed 2SM–APM with the same LES dataset from Lanzilao and Meyers (2024) that was used in section 2, and investigates the use of wake models to calculate C_P^* and C_T^*.

4.1 Relating the average APM and 2SM velocities

Combining the 2SM and APM approaches requires us to relate the average farm velocity used in the 2SM equations to the average lower-layer APM velocity within the farm. The former is defined as a straightforward average over the wind farm, so that

$$U_f = \frac{1}{H_f \Omega_f} \int_0^{H_f} \iint_{\Omega_f} u \mathrm{d}\Omega_f \mathrm{d}z, \tag{13}$$

where H_f is the height of the 2SM averaging volume, and Ω_f the planform area of the wind farm. In contrast, the APM predicts a horizontally filtered, height-averaged velocity field:

$$\langle \widetilde{u} \rangle_1 = \frac{1}{H_1 + \eta_1} \int_0^{H_1+\eta_1} \iint_{L_x \times L_y} G_\ell(x - x', y - y') u(x', y', z) \mathrm{d}x' \mathrm{d}y' \mathrm{d}z. \tag{3}$$

Averaging the APM variables over the farm can therefore only be done horizontally, so that

$$\overline{\langle \widetilde{u} \rangle}_1 = \frac{1}{\Omega_f} \iint_{\Omega_f} \langle \widetilde{u} \rangle_1 \mathrm{d}\Omega_f, \quad \overline{u}_1' = \frac{1}{\Omega_f} \iint_{\Omega_f} u_1' \mathrm{d}\Omega_f, \tag{14}$$

where the bars indicate farm-averaging for APM variables.

It's clear that the averages defined by equations 13 and 14 are not equivalent. Since the internal 2SM problem has to remain constant, the volume over which the farm average is defined should be independent of the mesoscale perturbation. However, the layer interface in the APM follows the flow streamlines, and its vertical displacement η_1 is part of the model state. This results in two different control volumes, as sketched in figure 3. Moreover, the APM velocity is filtered horizontally before being averaged, while the 2SM velocity is not.

https://doi.org/10.5194/wes-2026-14
Preprint. Discussion started: 13 February 2026

eawe european academy of wind energy
Open Access WIND ENERGY SCIENCE DISCUSSIONS

In this work, we neglect the filtering effects, thus presuming

$$\frac{1}{\Omega_f}\iint_{\Omega_f}\langle\widetilde{u}\rangle_1 \mathrm{d}\Omega_f \approx \frac{1}{\Omega_f}\iint_{\Omega_f}\langle u\rangle_1 \mathrm{d}\Omega_f. \tag{15}$$

Relating the 2SM and APM averages then only requires accounting for the discrepancy in the control volumes. Choosing $H_f = H_1$ makes these volumes as similar as possible, so that the remaining difference is solely due to the streamline displacement η_1. By then assuming that the velocity perturbation in the part of the APM layer above the 2SM volume scales with the velocity deficit within it, we find

$$(H_1+\overline{\eta}_1)\overline{u}'_1 \approx (H_1+\alpha\overline{\eta}_1)u'_f, \tag{16}$$

where α is a tuning parameter between 0 (no perturbation above the 2SM volume) and 1 (perfectly mixed APM layer), and u'_f is the 2SM-farm-averaged velocity deficit:

$$u'_f = U_f - U_1. \tag{17}$$

The 2SM-farm-averaged velocity can then be calculated from the APM state as

$$u'_f = \overline{u}'_1\frac{H_1+\overline{\eta}_1}{H_1+\alpha\overline{\eta}_1}, \quad U_f = U_1 + \overline{u}'_1\frac{H_1+\overline{\eta}_1}{H_1+\alpha\overline{\eta}_1}. \tag{18}$$

We tune α using the dataset of Lanzilao and Meyers (2024). We calculate APM states (u'_1, η_1) directly from the LES data by horizontally filtering the flow fields, advecting a set of points to find the height of the pliant surface between the APM layers, and height-averaging the flow. A detailed description of this procedure can be found in Devesse et al. (2024a). By relating the LES-based APM states set up this way to the U_f calculated directly from the LES, we find that $\alpha = 0.14$ gives good results.

4.2 Basic 2SM–APM coupling

We now focus on a fast 2SM–APM variant that will require solving the APM equations 5–8 only once, rather than at every iteration, thereby significantly speeding up the model.

4.2.1 Derivation

We begin by simplifying the notation. We can write the APM as a set of linear operators that transform the turbine forces to an APM state, so that

$$u'_1 = \mathcal{A}_u\left(\frac{\boldsymbol{f}}{h_1}\right), \quad \eta_1 = \mathcal{A}_\eta\left(\frac{\boldsymbol{f}}{h_1}\right), \quad p' = \mathcal{A}_p\left(\frac{\boldsymbol{f}}{h_1}\right), \tag{19}$$

where $\mathcal{A}_u$, $\mathcal{A}_\eta$, and $\mathcal{A}_p$ are linear operators that follow from the APM equations, and $\boldsymbol{f}$ is the turbine force. Note that this assumes that the direct turbine forces are the only perturbing forcing in the ABL. A more general approach would have to include the dispersive stresses and the increase in momentum flux as well. However, this does not change the following derivation conceptually.

https://doi.org/10.5194/wes-2026-14
Preprint. Discussion started: 13 February 2026

eawe european academy of wind energy
Open Access WIND ENERGY SCIENCE DISCUSSIONS

When using the APM with conventional wake model coupling methods, one of the largest computational costs is applying these operators $\mathcal{A}$, which involves a large linear system solve, at each step of the fixed-point iteration (Devesse et al., 2024b). In the classical APM, this iteration is needed because at each point in space, the local height-averaged farm force depends on the local velocity and layer thickness. However, these local variables are not relevant to the 2SM approach, as it only requires the average velocity over the farm. Since the goal of the 2SM–APM is to compute this quantity as cheaply as possible, including these local variations is an unnecessary cost. Therefore, we will assume that the distribution of the force in space, normalized by the total force $F/\overline{h}_1$, is independent of the APM state, so that

$$\frac{\boldsymbol{f}}{h_1} \approx \boldsymbol{\Pi}_f \frac{F}{H_1 + \overline{\eta}_1}, \tag{20}$$

where $\boldsymbol{\Pi}_f$ is the geometric footprint of the height-averaged force, and F is the total farm thrust (see eq. 2). If this footprint is indeed independent of the APM state, the model is reduced to a set of scalar equations:

$$\overline{u}_1' = a_u \frac{F}{H_1 + \overline{\eta}_1}, \quad \overline{\eta}_1 = a_\eta \frac{F}{H_1 + \overline{\eta}_1}, \tag{21}$$

where the coefficients a_u and a_η can be pre-computed:

$$a_u = \frac{1}{\Omega_f} \iint_{\Omega_f} \mathcal{A}_u\left(\boldsymbol{\Pi}_f\right) \mathrm{d}\Omega_f, \quad a_\eta = \frac{1}{\Omega_f} \iint_{\Omega_f} \mathcal{A}_\eta\left(\boldsymbol{\Pi}_f\right) \mathrm{d}\Omega_f. \tag{22}$$

We then arrive at a closed system of equations by computing the farm force F with equation 2, while relating U_f to the average APM perturbations using equation 18:

$$F = C_T^* \frac{U_f^2}{2} A_f, \tag{2}$$

$$U_f = U_1 + \overline{u}_1' \frac{H_1 + \overline{\eta}_1}{H_1 + \alpha \overline{\eta}_1}. \tag{18}$$

The linear system of equations 5–8 has to be inverted only once when calculating a_u and a_η, which greatly decreases the computational cost of the model.

The footprint $\boldsymbol{\Pi}_f$ can be chosen freely. In this work, we use the footprint of the farm forces obtained with a standalone wake model through equations 11–12 and scaled with the total farm force, so that

$$\widetilde{\boldsymbol{\Pi}}_f = \sum_k^{N_t} \left(C_{T,k}' A_k S_k^2 \boldsymbol{e}_k G_{\ell,k}\right) / F, \tag{23}$$

where the $C_{T,k}'$, S_k, $\boldsymbol{e}_k$, and F are calculated using a standalone wake model.

Including additional wind-farm perturbing forces, such as the induced dispersive and turbulent stresses, can be done by following the same steps as above. Since the APM operators are linear, the responses to different inputs can simply be summed up. If the perturbing forces scale with $F/\overline{h}_1$, as can be assumed for the dispersive stresses, this results in a modification of $\boldsymbol{\Pi}_f$

https://doi.org/10.5194/wes-2026-14
Preprint. Discussion started: 13 February 2026

eawe european academy of wind energy
Open Access WIND ENERGY SCIENCE DISCUSSIONS

when calculating a_u and a_η. However, including perturbing forces that scale differently, like the turbulent momentum flux in the upper layer, requires calculating additional coefficients for the scalar system of equations. We leave these complications to future work.

We briefly discuss how this 2SM–APM coupling relates to the coupling methods between the APM and underlying wake models developed in previous work. The most similar conventional method is the velocity matching (VM) approach developed by Devesse et al. (2024a), which calculates a background velocity that ensures that the wake model and the APM predict the same mesoscale velocity field at each point in the farm. This 2SM coupling imposes the same condition, but only on a farm average, so that the average farm velocity is the same in the internal and external problems (Nishino and Dunstan, 2020). Therefore, the 2SM–APM coupling can be seen as the VM method with just one degree of freedom for the background velocity.

4.3 Comparison to LES

To test the 2SM–APM approach, we validate the model with the LES results of Lanzilao and Meyers (2024) that were used in the previous sections. Like before, the farm coefficients are calculated using the neutral $H500$-$C0$-$G0$ case, which results in $C_T^* = 1.15$ and $C_p^* = 0.92$. This ensures that any errors introduced will come from the 2SM–APM coupling, and not from the estimation of the farm coefficients. The unperturbed background APM state is based on the precursor simulation driving each of the wind-farm simulations. We leave out the $H150$ cases, since the three-layer APM can not handle very shallow upper layer heights H_2 for the time being (Devesse et al., 2024a).

The numerical setup is the same as described in Devesse et al. (2024a). As discussed in the previous section, the APM operators $\mathcal{A}$ are solved using a Fourier-Galerkin method. To prevent the perturbations recycling through the periodic boundaries imposed by this method, we use the very large domain length of $L_x = 10\,000\mathrm{km}$ in the streamwise direction. In the spanwise direction, we take $L_y = 30\mathrm{km}$ in order to follow the LES results as closely as possible. The grid resolution is half of the horizontal filter length, so that $\Delta x = \Delta y = 500\mathrm{m}$.

The results are shown in figure 4, and the error statistics are listed in table 2. The fast 2SM–APM seems to perform well overall. The general trend is clear, and the global bias is fairly small. The root-mean square error (RMSE) across all analyzed cases is $4.7P_0$ (where P_0 is the power output of an isolated turbine), or 2.9% of the farm's installed capacity. This error is mostly due to the variance in the model errors. Furthermore, the model achieved the desired low computational cost, with each calculation taking roughly 2.7 seconds on a standard laptop, approximately 40 times longer than a wake model evaluation for the same farm.

To investigate the model's performance further, figure 5 shows the velocity deficit u_1' as predicted by the fast 2SM–APM model, compared to LES results. The model's accurate prediction of the average velocity is in part due to a cancellation of errors, as it over- and underpredicts the velocity at the front and back of the farm, respectively. However, this is not due to the 2SM simplifications, as earlier versions of the APM have similar errors (Devesse et al., 2024a). Improving the farm's parametrization by eg. including dispersive and turbulent stresses may improve this, but is out of the scope of this paper.

https://doi.org/10.5194/wes-2026-14
Preprint. Discussion started: 13 February 2026

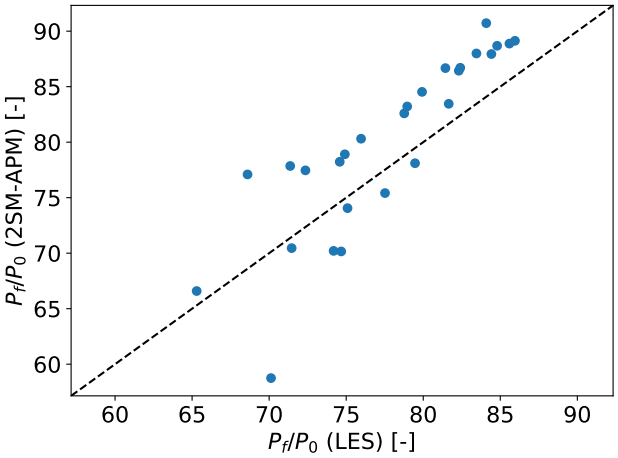

Figure 4. A comparison of farm power P_f as calculated by LES and the fast 2SM–APM model for 27 different CNBL cases from Lanzilao and Meyers (2024). The footprint of the height-averaged turbine forces is assumed to be constant, so that the linear system of APM equations only has to be solved once. The axes are normalized with the power output of a standalone turbine P_0.

Table 2. The root-mean square (RMSE), mean, and standard deviation (STD) of the error on farm power of all the models analyzed in the current paper for the LES dataset from Lanzilao and Meyers (2024). All values are scaled with the power output of a standalone turbine. Note that these three metrics are related, as $\text{RMSE}^2 = \text{Mean}^2 + \text{STD}^2$.

Model	RMSE [-]	Mean error [-]	Error STD [-]
U_f from LES, C_T^*, C_p^* from NBL LES	1.6	0.8	1.4
2SM–APM, C_T^*, C_p^* from NBL LES	4.7	2.3	4.1
2SM–APM, C_T^*, C_p^* from WM	6.0	-4.9	3.5
Farm-averaged PB	5.2	-3.5	3.8
Standalone WM	5.2	-1.1	5.1

4.3.1 Using a wake model to compute C_T^* and C_p^*

This section briefly demonstrates how a basic wake model can be used to calculate the farm thrust and power coefficients, and how this affects the model's performance. In essence, the process is the same as before, i.e. the standalone wake model is used to estimate U_f, P_f, and F, so that C_p^* and C_T^* can be calculated using equations 1 and 2. These can then by used by the 2SM–APM to predict the farm power output in different atmospheric conditions.

To calculate the farm power and thrust, we use a Gaussian wake model (Bastankhah and Porté-Agel, 2014) with the wake merging method of Lanzilao and Meyers (2021) and the turbulence-intensity model of Niayifar and Porté-Agel (2016). The

https://doi.org/10.5194/wes-2026-14
Preprint. Discussion started: 13 February 2026

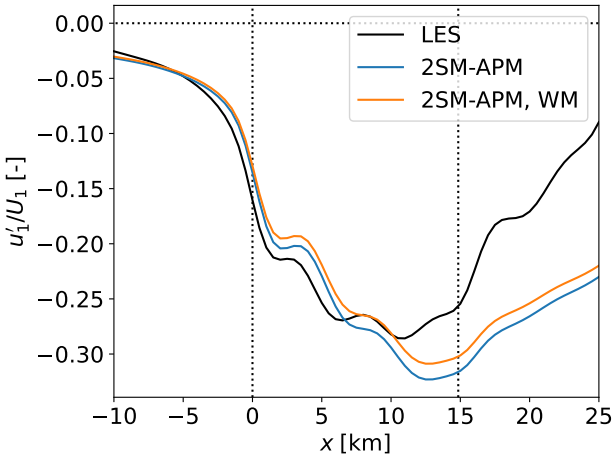

Figure 5. Lower-layer velocity deficit through the center of the farm as predicted by LES (black) and the fast 2SM–APM (blue, orange) for the case H500-$\Delta\theta$5-Γ4. The dotted lines denote the wind farm region. The blue and orange lines showing the 2SM–APM predictions were obtained with C_T^* values calculated using LES and a wake model, respectively.

wake model is not tuned, and is run with the parameters reported by the above authors. The turbines are mirrored to account for ground effects.

Accurately calculating U_f with a wake model requires more modeling effort than P_f and F (Devesse et al., 2024a). Since wake models typically only need to estimate the velocity at downstream turbine locations, they are not always optimized for velocity estimations in the near-wake and induction regions. If not properly accounted for, this can lead to large errors in the average velocity predictions. Therefore, we follow Devesse et al. (2024a) and include a turbine-induction model when estimating U_f (Troldborg and Meyer Forsting, 2017).

The farm-averaged velocity U_f is calculated by evaluating the wake model on a dense, evenly spaced grid over the whole 2SM averaging volume. This brute-force approach is computationally expensive, and a more efficient placement of the evaluation points would likely improve on it. However, as this section simply aims to demonstrate that this type of wake-model coupling can be done, we leave further investigations of how to best estimate U_f to future work.

The resulting C_T^* and C_p^* are 1.05 and 0.79, respectively. Both values are lower than those calculated from the neutral LES (1.15 and 0.92). This is mostly due to an error on U_f, as even with an induction model the farm-averaged velocity is overestimated (Devesse et al., 2024a).

With these coefficients, we now repeat the earlier validation using the LES dataset from Lanzilao and Meyers (2024). Figure 6 and table 2 show the resulting farm power predictions and error statistics, respectively, for both the 2SM–APM and the standalone wake model. Using the wake model to calculate C_T^* and C_p^* leads to a higher errors, mainly due to the consistent negative bias. Interestingly, the standalone wake model has a similar RMSE as the 2SM–APM despite not capturing any of the

https://doi.org/10.5194/wes-2026-14
Preprint. Discussion started: 13 February 2026

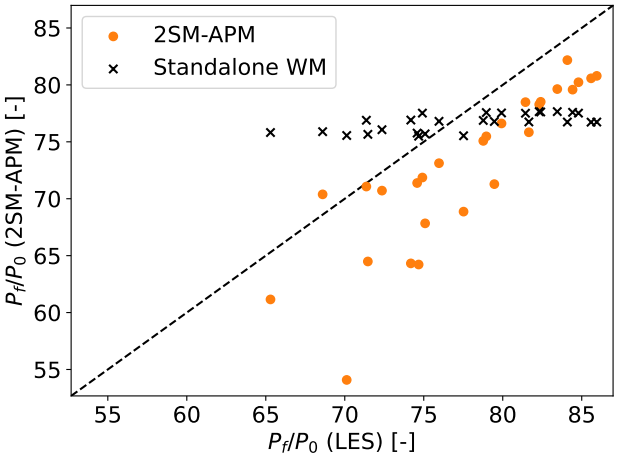

Figure 6. A comparison of farm power P_f as calculated by LES (x-axis), the fast 2SM–APM model (orange circles), and a standalone wake model (black crosses) for 27 different CNBL cases from Lanzilao and Meyers (2024). The farm coefficients C_T^* and C_p^* used by the 2AM–APM are calculated using the wake model. The axes are normalized with the power output of a standalone turbine P_0, as calculated using LES (horizontal) and the wake model (vertical).

power variations in the dataset, mostly because its mean error is very small. In comparison, the 2SM–APM have a higher bias, but a significantly lower variance.

To investigate the model behavior further, figure 5 shows the velocity perturbations predicted by the 2SM–APM. As a result of the lower C_T^* value, the model predicts smaller u_1' than before, leading to higher U_f. However, this is counteracted by the lower C_p^*, so that the resulting farm power predictions have a consistent negative bias.

5 Direct wake model coupling

The previous section treated C_T^* and C_p^* as known inputs from a wake model, and focused on improving the APM's cost and performance. However, calculating these coefficients with a wake model places requirements on said wake model's performance, and comes at a potentially significant computational cost. Therefore, we now apply the constant-footprint technique developed in the previous section to the pressure-based (PB) wake model coupling developed by Stipa et al. (2024a), resulting in a blockage-corrected model for farm power that does not require the explicit calculation of C_T^* and C_p^*.

This section first briefly derives the pressure-based wake model coupling technique. Afterwards, it applies the techniques developed in the previous section to eliminate the repeated APM operators. The resulting model is again validated using the dataset of Lanzilao and Meyers (2024).

https://doi.org/10.5194/wes-2026-14
Preprint. Discussion started: 13 February 2026

eawe european academy of wind energy
Open Access WIND ENERGY SCIENCE DISCUSSIONS

5.1 Derivation of the pressure-based coupling method

This section derives the equations for the pressure-based coupling method developed by Stipa et al. (2024a), by interpreting the APM as a correction model for CNBL effects. A similar but less thorough derivation has been made before by Devesse et al. (2024b).

A wake model estimates the turbine-scale velocity field $\boldsymbol{u}_{micro}$ by superposing turbine wake functions on a given background velocity $\boldsymbol{U}_b$, so that

$$\boldsymbol{u}_{micro} = \mathrm{WM}(\boldsymbol{U}_b), \tag{24}$$

where WM is the wake model operator.

The background velocity $\boldsymbol{U}_b$ is defined as being the velocity field that will result in the correct $\boldsymbol{u}_{micro}$ when the wakes are superimposed on it. In the absence of blockage and gravity-wave effects, this is simply the unperturbed velocity in the absence of the wind farm, so that $\langle\widetilde{\boldsymbol{U}_b}\rangle_1 = \boldsymbol{U}_1$. In contrast, when coupling a wake model to the APM, $\boldsymbol{U}_b$ has to ensure that

$$\langle\widetilde{\mathrm{WM}(\boldsymbol{U}_b)}\rangle_1 = \boldsymbol{U}_1 + \boldsymbol{u}'_1. \tag{25}$$

Devesse et al. (2024a) call this the *velocity matching* (VM) equation. This condition gives in an implicit equation for $\boldsymbol{U}_b$, and is related to using the pre-computed farm coefficients C_T^* and C_p^* when simplifying the APM–WM coupling using two-scale momentum theory, as discussed in the previous section. Similar to computing these farm coefficients, solving the VM equation for $\boldsymbol{U}_b$ is relatively expensive (Devesse et al., 2024b).

In order to find a computationally cheaper way to estimate $\boldsymbol{U}_b$, we decompose the filtered, height-averaged wake model operator into a wake and a correction component, so that

$$\langle\widetilde{\mathrm{WM}(\boldsymbol{U}_b)}\rangle_1 = \boldsymbol{U}_1 + \boldsymbol{u}'_{1,w} + \boldsymbol{u}'_{1,c}. \tag{26}$$

where the wake component $\boldsymbol{u}'_{1,w}$ is the filtered and height-averaged velocity deficit corresponding to the turbine wakes, as predicted by the wake model, and the correction component $\boldsymbol{u}'_{1,c}$ accounts for changes in the background velocity due to blockage. For sufficiently small perturbations, we can new assume

$$\langle\widetilde{\boldsymbol{U}_b}\rangle_1 = \boldsymbol{U}_1 + \boldsymbol{u}'_{1,c}. \tag{27}$$

Further using equation 25, the correction to the background velocity $\boldsymbol{u}'_{1,c}$ can then be found for a given APM state $\boldsymbol{u}'_1$ as

$$\boldsymbol{u}'_{1,c} = \boldsymbol{u}'_1 - \boldsymbol{u}'_{1,w}. \tag{28}$$

Therefore, the next step is to estimate $\boldsymbol{u}'_{1,w}$, i.e. the part of the APM velocity perturbation that corresponds to the wake deficit predicted by the wake model. Rather than obtaining this by averaging over the microscale velocity predicted by the wake model, we aim at finding an APM operator that allows us to make a faster direct estimation of $\boldsymbol{u}'_{1,w}$. Since conventional standalone wake models are designed to estimate the response of a neutral atmosphere to turbine forcing, we can reasonably take

$$\boldsymbol{u}'_{1,w} = \mathcal{A}_u^n\left(\frac{\boldsymbol{f}}{h_1}\right), \tag{29}$$

https://doi.org/10.5194/wes-2026-14
Preprint. Discussion started: 13 February 2026

eawe european academy of wind energy
Open Access WIND ENERGY SCIENCE DISCUSSIONS

where $\mathcal{A}_u^n$ is the APM operator for neutral conditions. The component $\boldsymbol{u}'_{1,c}$ can then be seen as a correction to neutral flow due to blockage effects, and is defined as

$$\boldsymbol{u}'_{1,c} = \mathcal{A}_u^c \left(\frac{\boldsymbol{f}}{h_1} \right), \tag{30}$$

where $\mathcal{A}_u^c$ is the APM operator for the difference between CNBL and neutral flow:

$$\mathcal{A}_u^c = \mathcal{A}_u - \mathcal{A}_u^n. \tag{31}$$

If this correction operator $\mathcal{A}_u^c$ is known, it can be used to directly predict $u'_{1,c}$ (and correspondingly U_b), without explicitly solving the velocity matching equation. To find $\mathcal{A}_u^c$, we first construct the neutral APM operator $\mathcal{A}_u^n$, since they are related through the above equation.

To find the neutral APM operator $\mathcal{A}_u^n$, we re-derive the APM for neutral flow. Doing so, the continuity and momentum equations remain unaltered. The only equation that changes is the pressure closure equation. In the absence of gravity waves, the pressure perturbations triggered by the farm are solely due to hydrodynamic effects, which are small compared to the buoyancy effects at typical wind farm length scales. This is demonstrated by the LES data of Lanzilao and Meyers (2024), where the pressure perturbations in the neutral cases are negligible compared to the CNBL simulations. Therefore, we take $p'_n = 0$.

We then easily find the model for the neutral component as equations 5–9 without the pressure term. For the sake of brevity, we only write the equations for the lower layer:

$$\boldsymbol{U}_1 \cdot \nabla_h \eta_{1,n} + H_1 \nabla_h \cdot \boldsymbol{u}'_{1,n} = 0, \tag{32}$$

$$\begin{aligned} \boldsymbol{U}_1 \cdot \nabla_h \boldsymbol{u}'_{1,n} \quad = \quad & f_c \mathbf{J} \cdot \boldsymbol{u}'_{1,n} + \nu_{t,1} \nabla_h^2 \boldsymbol{u}'_{1,n} \\ & + \frac{\mathbf{D}'}{H_1} \cdot \Delta_1^2 \boldsymbol{u}'_n - \frac{\mathbf{C}'}{H_1} \cdot \boldsymbol{u}'_{1,n} - \frac{\boldsymbol{T}_{h3,1} - \boldsymbol{T}_{h3,0}}{H_1^2} \eta_{1,n} \\ & + \frac{\widetilde{\boldsymbol{f}}}{H_1 + \eta_{1,n}}, \end{aligned} \tag{33}$$

$$p'_n = 0. \tag{34}$$

The equations for the correction operator $\mathcal{A}_u^c$ can then be found by simply substracting the above equations for the neutral model from the original APM continuity and momentum equations. Doing this results in

$$\boldsymbol{U}_1 \cdot \nabla_h \eta_{1,c} + H_1 \nabla_h \cdot \boldsymbol{u}'_{1,c} = 0, \tag{35}$$

$$\begin{aligned} \boldsymbol{U}_1 \cdot \nabla_h \boldsymbol{u}'_{1,c} \quad = \quad & f_c \mathbf{J} \cdot \boldsymbol{u}'_{1,c} + \nu_{t,1} \nabla_h^2 \boldsymbol{u}'_{1,c} \\ & + \frac{\mathbf{D}'}{H_1} \cdot \Delta_1^2 \boldsymbol{u}'_c - \frac{\mathbf{C}'}{H_1} \cdot \boldsymbol{u}'_{1,c} - \frac{\boldsymbol{T}_{h3,1} - \boldsymbol{T}_{h3,0}}{H_1^2} \eta_{1,c} \\ & - \frac{1}{\rho} \nabla_h p'_c, \end{aligned} \tag{36}$$

https://doi.org/10.5194/wes-2026-14
Preprint. Discussion started: 13 February 2026

eawe european academy of wind energy
Open Access WIND ENERGY SCIENCE DISCUSSIONS

$$p'_c = p' = \mathcal{A}_p\left(\frac{\boldsymbol{f}}{h_1}\right), \tag{37}$$

where we again only write the lower-layer equations for the sake of brevity. Note that for a given forcing $\boldsymbol{f}/h_1$, the pressure perturbation p' follows from equation 19 (based on the original APM operator $\mathcal{A}_p$), and is an input to equations 35–36.

We again define a simplified notation that expresses $\boldsymbol{u}'_{1,c}$ as the solution of the above system of equations:

$$\begin{aligned}\boldsymbol{u}'_{1,c} &= \mathcal{A}^c_{u,P}(p') \\ &= \mathcal{A}^c_{u,P}\left(\mathcal{A}_p\left(\frac{\boldsymbol{f}}{h_1}\right)\right),\end{aligned} \tag{38}$$

where the operator $\mathcal{A}^c_{u,P}$ represents the solution operator of equations 35–36 given p' as an input. Note that $\mathcal{A}^c_{u,P}(\mathcal{A}_p)$ thus defines $\mathcal{A}^c_u$ (eq. 31).

Finally, we have thus arrived at a closed system of equations, as through equation 38 we can calculate the change in background velocity for a given forcing $\boldsymbol{f}/h_1$. This allows us to again employ a fixed-point iteration, where $\boldsymbol{f}$ is calculated using the wake model, and the corresponding changes in h_1 and $\boldsymbol{u}_{1,c}$ are calculated using $\mathcal{A}_\eta$ and $\mathcal{A}^c_{u,P}(\mathcal{A}_p)$, respectively. The wake model then re-calculates the forces with the updated background velocity. This process is repeated until convergence.

The only remaining issue is that the input to the wake model requires a turbine-scale background velocity that is not height-averaged. The pressure-based coupling method therefore constructs a local background velocity for the wake model based on $\boldsymbol{u}'_{1,c}$ (Stipa et al., 2024a). Following the linearization of the APM, we write this background velocity $\boldsymbol{U}_b$ as the sum of the unperturbed velocity profile in the absence of the farm $\boldsymbol{U}_0$ and a perturbation around it, so that

$$\boldsymbol{U}_b(x,y,z) = \boldsymbol{U}_0(z) + \boldsymbol{u}_b(x,y) f_b(z), \tag{39}$$

where $\langle \boldsymbol{U}_0 \rangle_1 = \boldsymbol{U}_1$, and f_b is a shape function (we typically use a logarithmic function). The perturbation to the background velocity is then found by matching the height-averaged $u'_{1,c}$, so that

$$\boldsymbol{u}_b = \boldsymbol{u}'_{1,c}\left[\frac{1}{H_1+\eta_1}\int_0^{H_1+\eta_1} f_b \mathrm{d}z\right]^{-1}. \tag{40}$$

Stipa et al. (2024a) did not include the background component of the continuity equations (eq. 35) in their original coupling. However, the above derivation of the method shows that the whole APM operator should be split. These continuity equations add a parabolic behavior to the correction operator $\mathcal{A}^c_{u,P}$, so that the periodic boundary conditions imposed by the Fourier–Galerkin spectral method used to solve the original APM equations become inappropriate. However, since the closure equation for the internal gravity waves (eqs. 9–10) is not a part of the correction operator, we are free to use other numerical methods. Therefore, we solve equations 35–36 with a simple first-order explicit Euler marching scheme, with as inlet boundary conditions $\boldsymbol{u}'_{1,c}, \boldsymbol{u}'_{2,c}, \eta_{1,c}, \eta_{2,c} = 0$. To simplify this solver, we neglect Coriolis effects and the horizontal eddy viscosity, and assume $V_1 = V_2 = 0$.

https://doi.org/10.5194/wes-2026-14
Preprint. Discussion started: 13 February 2026

eawe european academy of wind energy
Open Access WIND ENERGY SCIENCE DISCUSSIONS

5.2 Farm-level pressure-based APM-WM coupling

We now apply the farm-averaging approach developed in the previous section to the PB coupling method. As discussed above, the background component of the APM velocity perturbation is given by

$$\boldsymbol{u}'_{1,c} = \mathcal{A}^c_{u,P}\left(\mathcal{A}_p\left(\frac{\boldsymbol{f}}{H_1+\eta_1}\right)\right). \tag{38}$$

By plugging in the constant footprint (eq. 20), we find that the average streamwise correction component is

$$\overline{u}'_{1,c} = a_{u,c}\frac{F}{H+\overline{\eta}_1}, \tag{41}$$

where the coefficient can be calculated as

$$a_{u,c} = \frac{1}{\Omega_f}\iint_{\Omega_f}\mathcal{A}^c_{u,P}\left(\mathcal{A}_p\left(\boldsymbol{\Pi}_f\right)\right)\mathrm{d}\Omega_f. \tag{42}$$

The average layer displacement $\overline{\eta}_1$ can be found through equation 21, as in the basic 2SM–APM.

Following the pressure-based coupling approach, we now use this $\overline{u}'_{1,c}$ to directly correct the background wind speed in a wake model. Since the above results only hold on a farm average, we assume a constant background over the farm:

$$U_b(z) = U_0(z) + \overline{u}_b f_b(z), \tag{43}$$

where the average background velocity scale $\overline{u}_b$ is found by matching $\overline{u}'_{1,c}$:

$$\overline{u}_b = \overline{u}'_{1,c}\left[\frac{1}{H_1+\overline{\eta}_1}\int_0^{H_1+\overline{\eta}_1} f_b\mathrm{d}z\right]^{-1}. \tag{44}$$

The wake model can then be used to calculate F and P_f, closing the system of equations:

$$F = \sum_k^{N_t}\frac{1}{2}C'_{T,k}S_k^2A_k, \tag{45}$$

$$P_f = \sum_k^{N_t}\frac{1}{2}\rho C'_{p,k}S_k^3A_k, \tag{46}$$

where the turbine coefficients and disk velocities are calculated using a wake model with the background velocity defined in equation 43.

We solve the final system of equations (41, 21, 45, 46) using a fixed-point iteration solver with a relaxation factor of 0.7, as is done for the classical APM and the 2SM–APM developed in the previous section.

The advantages of this approach compared to the 2SM–APM coupling derived in the previous section are similar to the advantages of PB coupling compared to the VM method. It places no requirements on the wake model, and does not need to calculate C_T^* and C_p^*. While this coupling no longer explicitly uses any of the results from 2SM theory, it implicitly makes the same assumption that farm power calculations only need the average wind speed within a farm.

https://doi.org/10.5194/wes-2026-14
Preprint. Discussion started: 13 February 2026

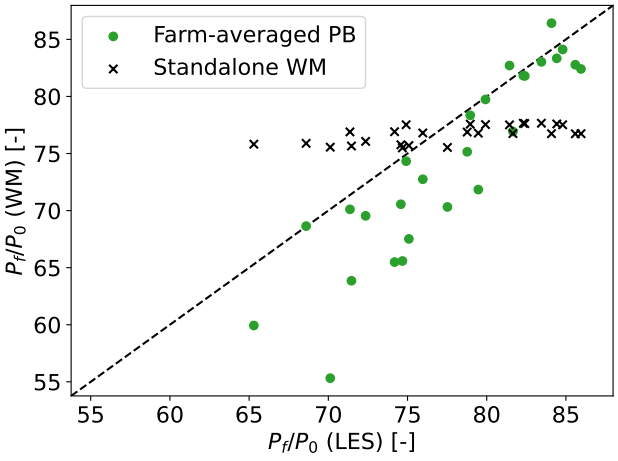

Figure 7. Farm power as calculated by LES (x-axis) and wake model (y-axis), both standalone (black crosses) and with farm-average pressure-based blockage coupling (green circles). The axes are normalized with the power output of a standalone turbine P_0, as calculated using LES (horizontal) and the wake model (vertical).

5.2.1 Comparison to LES

We again validate this approach using the LES cases from the dataset by Lanzilao and Meyers (2024) used throughout this work. The numerical setup for the $\mathcal{A}_p$ operator is the same as in section 4.3. The correction operator $\mathcal{A}^c_{u,P}$ can use a smaller numerical domain, since its solver does not require periodic boundary conditions. Here, we use the same spanwise $L_y = 30\text{km}$ as before, but take a shorter streamwise $L_x = 43\text{km}$, placing the solver's inlet at the same upstream distance of the farm as the LES, i.e. 18km. We use the same wake model as in section 4.3.1.

The results are shown in figure 7, and the error statistics are listed in table 2. The general trend is visible, despite some scatter and a consistent negative bias. Overall, the wake model and the farm-level PB coupled model have the same RMSE on power of $5.2P_0$, or 3.3% of the farm's installed capacity, with the farm-averaged PB model having a lower error variance but larger bias. The computational cost is the same as before, as the pressure component operator and wake model evaluations have a negligible cost.

As shown above, the pressure-based coupling can be derived as a correction to an NBL base state. With that in mind, figure 8 shows the difference in farm power between the coupled and standalone wake model, compared to the farm power differences between the CNBL and the neutral LES reference simulation, i.e. $H500$-$\Delta\theta 0$-$\Gamma 0$. It's clear that the farm-average coupling performs decently in the role of a blockage-correction model. The error on this power difference is similar to the error on the farm powers shown in figure 7, which indicates that the farm-averaged PB model's bias is mostly due to an overprediction of blockage losses.

https://doi.org/10.5194/wes-2026-14
Preprint. Discussion started: 13 February 2026

eawe european academy of wind energy
Open Access WIND ENERGY SCIENCE DISCUSSIONS

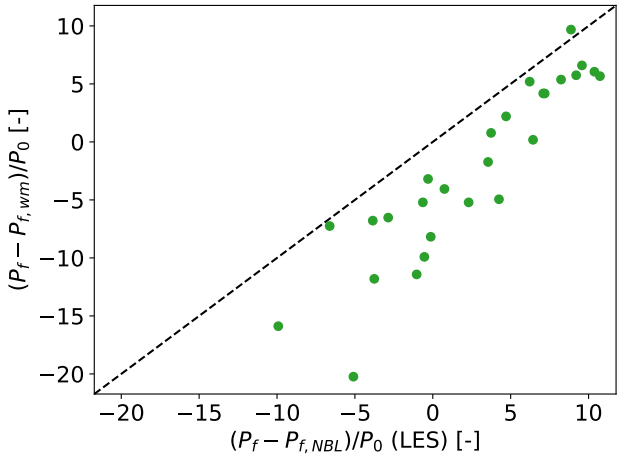

Figure 8. Difference between farm power in CNBL and NBL conditions as calculated by LES (x-axis) and wake model with farm-average pressure-based blockage coupling (y-axis). The axes are normalized with the power output of a standalone turbine P_0, as calculated using LES (horizontal) and the wake model (vertical).

6 Conclusions

Two-scale momentum (2SM) theory offers an interesting new way of including mesoscale effects in wind farm power predictions. Using results from Lanzilao and Meyers (2024), its core hypothesis was validated for steady-state idealized CNBL conditions. Building on that, this paper developed two ways to combine it with an atmospheric perturbation model (APM) to speed up farm power calculations. This speed-up is possible because according to the 2SM hypothesis, only the average velocity within a farm U_f is needed to compute the farm's force and power output. Since local fluctuations in the turbine forcing are therefore not relevant, the spatial distribution of the forces is assumed to be constant and independent of the APM state. Combined with the linearity of the APM, this transforms the APM's governing equations into a system of algebraic equations, which are trivial to solve numerically.

The first version of the 2SM–APM uses the APM as a mesoscale model to obtain the average velocity within the farm, and uses the 2SM farm coefficients C_T^* and C_p^* to calculate the turbine forces and power output. This basic coupling method is similar to the velocity matching method developed in by Devesse et al. (2024a), as it matches the average farm velocity between the meso- and turbine scales. It performs well, and predicts the farm power in CNBL conditions accurately for known C_T^* and C_p^*.

The second model developed in this paper avoids the use of C_T^* and C_p^* by coupling directly to a wake model. To this end, it applies the farm-averaging approach to the pressure-based wake model coupling method of Stipa et al. (2024a). Based on a rigorous derivation of this method, we show that it can also be interpreted as a model to correct neutral flow results for CNBL effects. The model performs well in this role, and can predict the effects of blockage and gravity waves on farm power, albeit with a consistent bias.

https://doi.org/10.5194/wes-2026-14
Preprint. Discussion started: 13 February 2026

Both models presented here achieve a lower variance in the error on their power predictions compared to a standalone wake model, at the cost of a larger bias. Tuning the underlying wake models could address this, as both the wake spreading coefficients and the farm-averaged power and thrust coefficients can be optimized. The low computational cost of the models allows this tuning to directly incorporate large operational datasets. We believe this is a promising area of further research that will facilitate the model's adoption by the wind energy industry and community.

Code availability. The models developed in this paper have been implemented in the open-source code WAYVE (Devesse et al., 2023), and will be published alongside with the final version of this paper.

Author contributions. KD and JM jointly derived the 2SM–APM couplings and set up the validation studies. KD performed code implementations and carried out the simulations. KD and JM jointly wrote the manuscript.

Competing interests. One of the (co-)authors is a member of the editorial board of Wind Energy Science. The authors have no other competing interests to declare.

Acknowledgements. The authors thank Frederik Aerts for insightful discussions on combining the 2SM and APM approaches. This research has been supported by the Energy Transition Fund of the Belgian Federal Public Service for Economy, SMEs, and Energy (FOD Economie, K.M.O., Middenstand en Energie), by the European Union Horizon Europe Framework programme (HORIZON-CL5-2021-D3-03-04) under grant agreement no. 101084205, and by Project Cloud4Wake, funded by Vlaamse Agentschap Innoveren & Ondernemen (VLAIO) under the Blue Cluster cSBO programme (Contract number HBC.2022.0549)

https://doi.org/10.5194/wes-2026-14
Preprint. Discussion started: 13 February 2026

eawe european academy of wind energy
Open Access WIND ENERGY SCIENCE DISCUSSIONS

References

Allaerts, D. and Meyers, J.: Boundary-layer development and gravity waves in conventionally neutral wind farms, Journal of Fluid Mechanics, 814, 95–130, https://doi.org/10.1017/jfm.2017.11, 2017.

Allaerts, D. and Meyers, J.: Gravity Waves and Wind-Farm Efficiency in Neutral and Stable Conditions, Boundary-Layer Meteorology, 166, 269–299, https://doi.org/10.1007/s10546-017-0307-5, 2018.

Allaerts, D. and Meyers, J.: Sensitivity and feedback of wind-farm-induced gravity waves, Journal of Fluid Mechanics, 862, 990–1028, https://doi.org/10.1017/jfm.2018.969, 2019.

Bastankhah, M. and Porté-Agel, F.: A new analytical model for wind-turbine wakes, Renewable Energy, 70, 116–123, https://doi.org/10.1016/j.renene.2014.01.002, 2014.

Bleeg, J., Purcell, M., Ruisi, R., and Traiger, E.: Wind farm blockage and the consequences of neglecting its impact on energy production, Energies, 11, https://doi.org/10.3390/en11061609, 2018.

Centurelli, G., Vollmer, L., Schmidt, J., Dörenkämper, M., Schröder, M., Lukassen, L. J., and Peinke, J.: Evaluating Global Blockage engineering parametrizations with LES, Journal of Physics: Conference Series, 1934, 012 021, https://doi.org/10.1088/1742-6596/1934/1/012021, 2021.

Devesse, K., Lanzilao, L., Allaerts, D., Jamaer, S., and Meyers, J.: Wind-fArm gravitY-waVe and blockagE code, https://doi.org/10.48804/XMNVVY, 2023.

Devesse, K., Lanzilao, L., and Meyers, J.: A meso–micro atmospheric perturbation model for wind farm blockage, Journal of Fluid Mechanics, 998, A63, https://doi.org/10.1017/jfm.2024.868, 2024a.

Devesse, K., Stipa, S., Brinkerhoff, J., Allaerts, D., and Meyers, J.: Comparing methods for coupling wake models to an atmospheric perturbation model in WAYVE, Journal of Physics: Conference Series, 2767, 092 079, https://doi.org/10.1088/1742-6596/2767/9/092079, 2024b.

Du, B., Ge, M., Li, X., and Liu, Y.: A Meso-Microscale Coupled Wind Farm Parameterization, Boundary-Layer Meteorology, 191, 35, https://doi.org/10.1007/s10546-025-00928-7, 2025.

Gill, A. E.: Atmosphere-Ocean Dynamics, International geophysics series 30, Academic Press, San Diego, USA, ISBN 0122835204, 1982.

Kirby, A., Nishino, T., and Dunstan, T. D.: Two-scale interaction of wake and blockage effects in large wind farms, Journal of Fluid Mechanics, 953, 1–28, https://doi.org/10.1017/jfm.2022.979, 2022.

Kirby, A., Nishino, T., Lanzilao, L., Dunstan, T. D., and Meyers, J.: Turbine- and farm-scale power losses in wind farms: an alternative to wake and farm blockage losses, Wind Energy Science, 10, 435–450, https://doi.org/10.5194/wes-10-435-2025, 2025.

Lanzilao, L. and Meyers, J.: Set-point optimization in wind farms to mitigate effects of flow blockage induced by atmospheric gravity waves, Wind Energy Science, 6, 247–271, https://doi.org/https://doi.org/10.5194/wes-6-247-2021, 2021.

Lanzilao, L. and Meyers, J.: Effects of self-induced gravity waves on finite wind-farm operations using a large-eddy simulation framework, Journal of Physics: Conference Series, 2265, https://doi.org/10.1088/1742-6596/2265/2/022043, 2022.

Lanzilao, L. and Meyers, J.: An Improved Fringe-Region Technique for the Representation of Gravity Waves in Large Eddy Simulation with Application to Wind Farms, Boundary-Layer Meteorology, 186, 567–593, https://doi.org/10.1007/s10546-022-00772-z, 2023a.

Lanzilao, L. and Meyers, J.: A reference database of wind-farm large-eddy simulations for parametrizing effects of blockage and gravity waves, https://doi.org/10.48804/L45LTT, 2023b.

https://doi.org/10.5194/wes-2026-14
Preprint. Discussion started: 13 February 2026

Lanzilao, L. and Meyers, J.: A parametric large-eddy simulation study of wind-farm blockage and gravity waves in conventionally neutral boundary layers, Journal of Fluid Mechanics, 979, A54, https://doi.org/10.1017/jfm.2023.1088, 2024.

Maas, O.: From gigawatt to multi-gigawatt wind farms: wake effects, energy budgets and inertial gravity waves investigated by large-eddy simulations, Wind Energy Science, 8, 535–556, https://doi.org/10.5194/wes-8-535-2023, 2023a.

Maas, O.: Large-eddy simulation of a 15 GW wind farm: Flow effects, energy budgets and comparison with wake models, Frontiers in Mechanical Engineering, 9, 1–23, https://doi.org/10.3389/fmech.2023.1108180, 2023b.

Meyers, J., Bottasso, C., Dykes, K., Fleming, P., Gebraad, P., Giebel, G., Göçmen, T., and van Wingerden, J.-W.: Wind farm flow control: prospects and challenges, Wind Energy Science, 7, 2271–2306, https://doi.org/10.5194/wes-7-2271-2022, 2022.

Niayifar, A. and Porté-Agel, F.: Analytical Modeling of Wind Farms: A New Approach for Power Prediction, Energies, 9, 741, https://doi.org/10.3390/en9090741, 2016.

Nishino, T. and Dunstan, T. D.: Two-scale momentum theory for time-dependent modelling of large wind farms, Journal of Fluid Mechanics, 894, https://doi.org/10.1017/jfm.2020.252, 2020.

Porté-Agel, F., Bastankhah, M., and Shamsoddin, S.: Wind-Turbine and Wind-Farm Flows: A Review, Boundary-Layer Meteorology, 174, 1–59, https://doi.org/10.1007/s10546-019-00473-0, 2020.

Smith, R. B.: Gravity wave effects on wind farm efficiency, Wind Energy, 13, 449–458, https://doi.org/10.1002/we.366, 2010.

Stipa, S., Ajay, A., Allaerts, D., and Brinkerhoff, J.: The multi-scale coupled model: a new framework capturing wind farm-atmosphere interaction and global blockage effects, Wind Energy Science, 9, 1123–1152, https://doi.org/10.5194/wes-9-1123-2024, 2024a.

Stipa, S., Ajay, A., Allaerts, D., and Brinkerhoff, J.: TOSCA – an open-source, finite-volume, large-eddy simulation (LES) environment for wind farm flows, Wind Energy Science, 9, 297–320, https://doi.org/10.5194/wes-9-297-2024, 2024b.

Stipa, S., Ajay, A., and Brinkerhoff, J.: The actuator farm model for large eddy simulation (LES) of wind-farm-induced atmospheric gravity waves and farm–farm interaction, Wind Energy Science, 9, 2301–2332, https://doi.org/10.5194/wes-9-2301-2024, 2024c.

Troldborg, N. and Meyer Forsting, A. R.: A simple model of the wind turbine induction zone derived from numerical simulations, Wind Energy, 20, 2011–2020, https://doi.org/10.1002/we.2137, 2017.

Van der Laan, M. P., García-Santiago, O., Kelly, M., Meyer Forsting, A., Dubreuil-Boisclair, C., Sponheim Seim, K., Imberger, M., Peña, A., Sørensen, N. N., and Réthoré, P.-e.: A new RANS-based wind farm parameterization and inflow model for wind farm cluster modeling, Wind Energy Science, 8, 819–848, https://doi.org/10.5194/wes-8-819-2023, 2023.